Research Article | Vol. 10, No. 6 | 1 Jun 2019 | BIOMEDICAL OPTICS EXPRESS 2674
Biomedical Optics EXPRESS

Impact of optical tissue clearing on the Brillouin signal from biological tissue samples

Rafael J. Jiménez Riobóo,[1] Manuel Desco,[2,3,4,5,*] and María Victoria Gómez-Gaviro[2,3,4]

[1]*Instituto de Ciencia de Materiales de Madrid ((ICMM), Consejo Superior de Investigaciones Científicas (CSIC), C/ Sor Juana Inés de la Cruz, 3, 28049 Madrid, Spain*
[2]*Instituto de Investigación Sanitaria Gregorio Marañón (IiSGM), Doctor Esquerdo 46, 28007 Madrid, Spain*
[3]*Departamento de Bioingeniería e Ingeniería Aeroespacial, Universidad Carlos III de Madrid, 28911 Leganés, Spain*
[4]*Centro de Investigación Biomédica en Red de Salud Mental (CIBERSAM), 28029 Madrid, Spain*
[5]*Centro de Investigaciones Cardiovasculares (CNIC), Melchor Fernández Almagro, 28029 Madrid, Spain*
**desco@hggm.es*

Abstract: Brillouin spectroscopy is a well-established technology in condensed matter physics to characterize the mechanical properties of inert materials, and it has been extended very recently to the study of biological samples. Transparency is beneficial for samples to be properly analyzed by Brillouin spectroscopy. Here, we explored the efficacy of optical tissue clearing techniques to improve the acquisition of Brillouin spectra from biological tissues in order to analyze their biomechanical properties. We describe the first application of Brillouin scattering to optically cleared biological tissues with CUBIC protocol. We conclude that, within the range of error, tissue clearing does not modify the mechanical properties of the studied biological tissues.

1. Introduction

Brillouin microscopy is a promising non-invasive and non-destructive technology under commercial development at present. The technique enables researchers to characterize the mechanical properties of both, inert samples and, more recently, biological tissues [1–6]. Non transparent samples can limit the possibilities of using Brillouin spectroscopy [7] and therefore, the study of biological samples has been limited to cultured cells and naturally transparent tissues.

The study of living biological samples has been made possible with VIPAs (Virtually Imaged Phased Arrays), which are new spectrometers that allow fast spectral measurements [8]. The mechanical properties of the extracellular matrix, nucleoli and cytoplasm have been analyzed in live plant cells [9] and in human umbilical vein endothelial cells with Brillouin [10]. In this context, ex vivo human epithelial tissue was the first biomedical application of confocal Brillouin and Raman microscopy [3]. In animal models, zebrafish larvae have been used to elaborate the mechanical mapping of the spinal cord growth in vivo [11].

In addition, the development of Brillouin light scattering microscopy has made it possible to bring biomechanics closer to the clinics. Medical diagnostics applications of this new technology are being investigated. Clinical trials are already ongoing in the field of ophthalmology (ClinicalTrials.gov, Identifier: NCT02118922). Brillouin has also been used to demonstrate ability to detect features associated with bacterial meningitis [12].

Different optical tissue clearing protocols have been developed recently to obtain 3D tissue images at single cell resolution [13,14]. Tissue clearing techniques make the tissues

#356450 https://doi.org/10.1364/BOE.10.002674
Journal © 2019 Received 3 Jan 2019; revised 24 Feb 2019; accepted 3 Mar 2019; published 2 May 2019

Biomedical Optics EXPRESS

transparent reducing the opacity by lipid removal. Sample opacity considerably limits the laser light penetration depth due to differences in the refractive indices in the tissue (opacity of the tissue) and the resulting light scattering effects. These limitations are overcome by tissue clearing, thereby enabling the study of detailed 3D structures. Micro-Brillouin has been applied to mouse brain to analyze amyloid-beta plaques in transgenic animals and in Alzheimer's disease brains [6,15]. We analyzed different areas of brain and heart mouse samples optically cleared with the CUBIC (clear, unobstructed brain imaging cocktails and computational analysis) protocol [16–18] and compared them with uncleared tissue. The aim of this work is precisely to show the effects, if any, of the clearing process in Micro-Brillouin experiments, which are the key for assessing the elastic properties of biological tissue. Any other effects due to the tissue clearing technique have not been addressed. In so far we have focused our attention to the position and width of the Brillouin peaks in different samples, treated and not treated. We used 20X and 50X magnification objectives to acquire micro-Brillouin spectra from different regions of the sample. Heart samples showed more homogeneity than brain samples even under untreated conditions, but the quality of the Brillouin spectrum was further improved after tissue clearing.

Here we present a novel approach to the study of tissue biomechanical properties that combines optical tissue clearing protocols and Brillouin spectroscopy.

2. Material and methods

2.1 Biological samples preparation

Adult male mice (n = 3) were anesthetized with intraperitoneal administration of 80 mg/kg and 2 mg/kg of Ketamine/Xylazin, respectively. To obtain the brain and heart tissues, the chest cavity of the animal was opened and mice were transcardially perfused with 20 ml of ice cold phosphate buffered solution (PBS) followed by 50 ml of 4% paraformaldehyde (PFA). Hearts and brains were dissected and post-fixed in 4% PFA at 4°C for at least 12 h [19,20]. Then the organs were washed with PBS and cleared with the CUBIC-clearing reagents [21]. To clear the mouse brains and hearts, they were immersed in CUBIC clearing reagent 1 (R1) for 7 days in a shaker at 80 rpm at 37°C. R1 consists of 2.5 g of urea, 2.5 g of N,N,N,N-tetrakis 2-hydroxy-propyl, 25% ethilenediamine and 15% Triton X-100 in 3.5 mL of water. After the first three days, R1 was replaced with fresh R1. Then, tissues were washed as above with PBS-T (containing 0.1% Triton X-100 and immersed in CUBIC clearing reagent 2 (R2) for a maximum of 24 h at 37°C, with shaking at 80 rpm. R2 consists of 5 g of sucrose, 2.5 g of urea and 1 g of triethanolamine in 1.5mL of water. The protocol is summarized in Fig. 1.

Uncleared and cleared tissue were sliced transversally into 70 μm cross-sections with a vibratome (Campden Instruments). Slices were placed on a microscope slide. DAKO mounting solution was applied, and the sample was covered with a coverslip.

Biomedical Optics EXPRESS

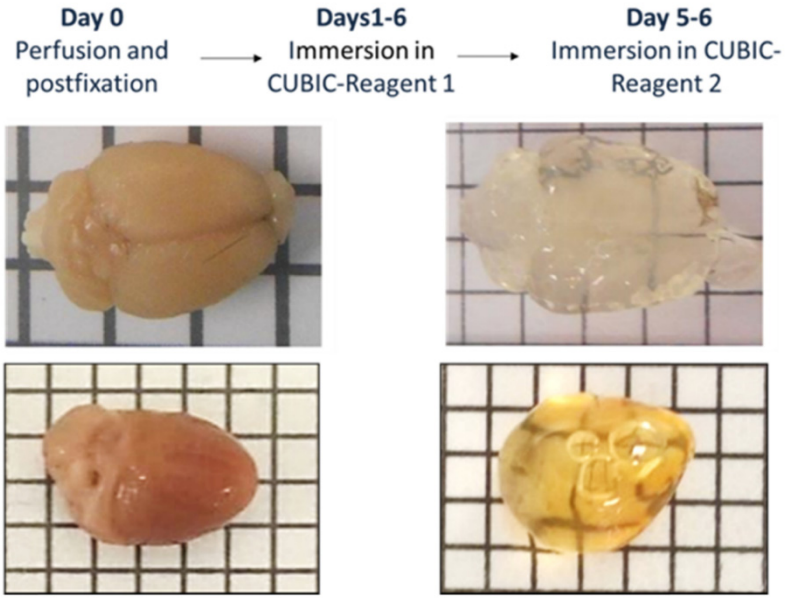

Fig. 1. CUBIC protocol for clearing mouse heart and brain. Animals were perfused with 4% PFA and brain and heart were dissected out. The CUBIC method was used to clear the tissues and a vibratome was used to slice the tissue. On the superior part the steps of the protocol are described. The superior pictures represent, on the left, an unclear (left) and cleared (right) mouse brain and in the inferior part an unclear (left) and cleared (right) mouse are represent.

2.2 Brillouin spectroscopy

High resolution micro-Brillouin spectroscopy (HRmBS) was performed with the aid of a home modified reflected light Olympus BX51 microscope with three different objectives: X10, X20 and X50. The experimental setup [22] is schematically shown in Fig. 2. Brillouin spectra were recorded using a Sandercock 3 + 3 Pass Tandem Fabry-Pérot interferometer as Brillouin spectrometer [23] and the monochromatic light source used was a DPPS laser working at a wavelength (λ_0) of 532 nm. Brillouin microscopy used typically a 1.9 mW laser beam to obtain the HRmBS spectra.

Micro-Brillouin spectroscopy implies that information can be only obtained in backscattering geometry, thus being sensitive to the refractive index. An additional drawback of the backscattering geometry is that, in principle, there is no coupling with shear acoustic modes [24]. The acoustic wave vector for backscattering geometry is $q^{180} = [4\ \pi\ n] / \lambda_0$, and hence n-dependent [25]. The hypersonic sound propagation velocity (v) is obtained from the relation between the Brillouin frequency shift (f^{180}) and q^{180}, and expressed as $v = (2\ \pi\ f^{180}) / q^{180}$. Thus, the hypersonic velocity reads: $v = f^{180}\ \lambda_0 / 2n$. It is then straightforward to assess the corresponding elastic constant if the mass density of the sample (ρ) and its refractive index are known. $c = \rho\ v^2$."

3. Results and discussion

3.1 CUBIC clearing in brain and cardiac mouse tissue

Clearing protocols have been optimized to clear whole brain and heart [19–21]. Here, we used an optimized CUBIC protocol that partially removes the lipids causing tissue opacity, the Reagent 1 being responsible for this effect. How this reagent affects the tissue properties is still unclear. The size of the samples is slightly modified by the reagents used but cellular and subcellular structure is maintained [19–21] (Fig. 1). It has been described that Brillouin measurements depend on the fluid content of the material [26]. As CUBIC protocol removes

Biomedical Optics EXPRESS

partially lipids we measured Brillouin frequency of the CUBIC-reagent 1 responsible of that with CUBIC-R1 after tissues incubation (Table 1).

Table 1. Brillouin spectroscopy on clearing reagents. Distilled H2O, fresh Reagent 1 (R1) and R1 measurement after heart and brain clearing. 90A scattering geometry and backscattering geometry were used simultaneously in order to asses hypersonic sound velocity and refractive index [27]. For comparison, the refractive index was also measured with a standard Abbe refractometer (nA).

	f90A (GHz)	f180 (GHz)	v (m/s)	n (Brillouin/nA)
H2O	4.05	7.49	1522	1.31/1.33
R1	4.65	9.20	1752	1.40/1.41
R1 heart	4.66	9.24	1752	1.40/1.41
R1 brain	4.68	9.29	1760	1.40/1.41

3.2 Brillouin measurements for cleared tissue

Since we were interested in changes in the elastic properties of homogeneous tissues, we focused our attention onto the differences in Brillouin frequency shift for different areas of the studied tissues. Figure 2(a) shows an actual picture of the HRmBS used and Fig. 2(b) shows the schematics setup.

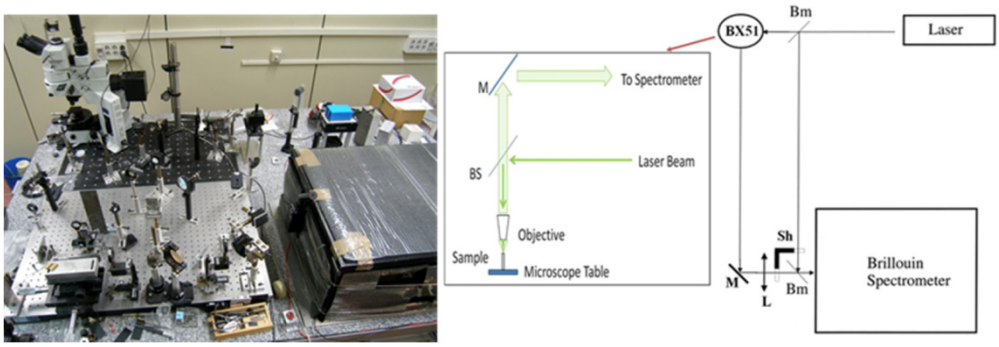

Fig. 2. Brillouin spectroscopy set-up. (a) Picture of the Brillouin light scattering apparatus with the possibility of performing classical as well as micro Brillouin spectroscopy. (b) Schematics of the micro-Brillouin set-up. Laser light is directed into a modified reflected light microscope. Backscattered light is collected and the Rayleigh light is chopped with a mechanical shutter in order to protect the photomultiplier.

First, we tested the suitability of the clearing protocols in order to improve the quality of the Brillouin peaks in different tissues without altering their elastic response. For this purpose, two different microscope objectives were used (X20 and X50). As shown in Figs. 3(a)-3(f), clearing the brain tissue enabled us to obtain narrower and more intense peaks, Table 2.

Biomedical Optics EXPRESS

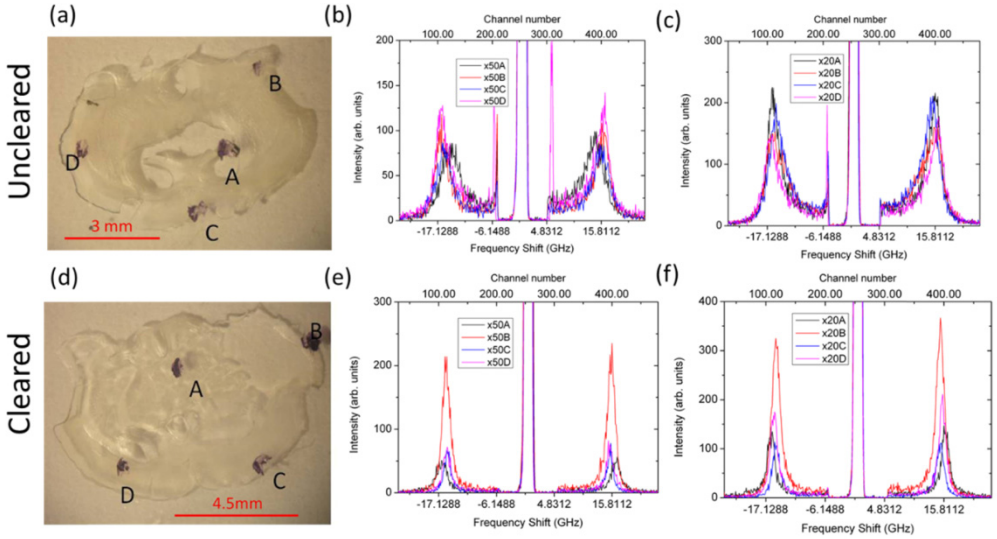

Fig. 3. Effect of brain tissue clearing on Brillouin spectra. (a-c) Optical image (a) and Brillouin scattering spectrum (b, c) of uncleared brain sections. (d-f) Optical image (d) and Brillouin scattering spectra (e,f) of cleared brain sections. Different colours represent different tissue areas as indicated in A, B, C and D. 50X (b, e) and 20X (c, f) objectives were used.

The spectra are shown in channel number and Brillouin frequency shift. All the experimental conditions are the same for all the spectra, thus allowing direct comparison.

Table 2. Quantifications of Brillouin spectroscopy brain sections. Frequency shift (f) and Half Width at Half Maximum (Γ) of the Brillouin peak derived from fit analysis of the spectra in the linear scan. NC Non cleared, C: cleared.

	A f /Γ GHz	B f / Γ GHz	C f / Γ GHz	D f / Γ GHz	Mean Value f / Γ GHz
NCX20	15.11 /2.5	15.56 /2.44	15.17 /1.81	16.30 /1.60	15.54 /2.08
CX20	16.13 /0.81	15.20 /0.89	15.17 /0.82	15.57 /0.76	15.52 /0.82
NCX50	14.53 /2.37	16.26 /1.54	15.82 /1.95	16.21 /1.53	15.71 /1.85
CX50	16.56 /0.86	15.71 /0.87	15.47 /0.66	15.51 /0.82	15.81 /0.80

Similarly, clearing cardiac tissue resulted in improved Brillouin signal, as shown in Figs. 4(a)-4(h) and Table 3.

Biomedical Optics EXPRESS

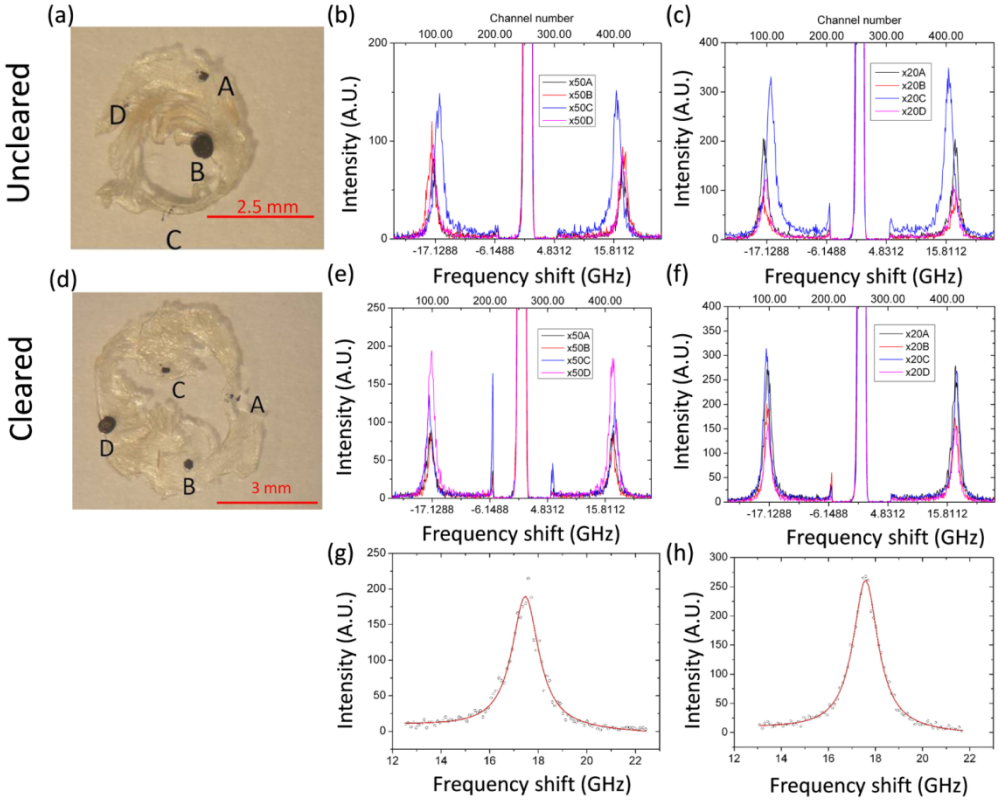

Fig. 4. Effect of heart tissue clearing on Brillouin spectra. (a-c) Optical image (a) and Brillouin scattering spectrum (b, c) of uncleared heart sections. (d-f) Optical image (d) and Brillouin scattering spectrum (e, f) of cleared heart sections. Different colors represent different tissue areas as indicated in A, B, C and D. 50X (b, e) and 20X (c, f) objectives were used. (g, h) Result of a non linear squares fit (red line) of the experimental data (circles) using a simple lorentzian function plus a suited background function for the anti-stokes side of the Brillouin spectrum. (g) not cleared heart sample tissue and (h) cleared heart sample tissue.

Table 3. Quantifications of Brillouin spectroscopy heart sections. Frequency shift (f) and Half Width at Half Maximum (Γ) of the Brillouin peak derived from fit analysis of the spectra in the linear scan. NC Not cleared, C: cleared.

	A f / Γ GHz	B f / Γ GHz	C f / Γ GHz	D f / Γ GHz	Mean Value f / Γ GHz
NCX20	17.58 /0.68	17.77 /1.05	16.38 /0.90	17.36 /0.72	17.27 /0.84
CX20	17.38 /0.76	17.42 /0.65	17.62 /0.64	17.36 /0.71	17.45 /0.69
NCX50	17.47 /0.68	17.80 /0.82	16.46 /0.83	17.46 /0.69	17.30 /0.75
CX50	17.34 /0.73	17.28 /0.60	17.69 /0.69	17.28 /0.74	17.40 /0.69

In a second step, we focused our attention on a defined region of cleared heart tissue in order to test the sensitivity of the HRmBS to different regions of the same tissue (Figs. 5(a)-5(e)). In these experiments only the objective X20 was used. Different regions of heart tissue (I and II in Fig. 5(a)) were investigated. These regions are individually shown in Figs. 5(b) and 5(c). In region I (Fig. 5(b)), two different measurements were obtained, one from the border of the sample (purple circle A, corresponding to the epicardial layer) myocardium) and a second one from its the middle (purple circle B, myocardial layer), as depicted in the micrograph (objective X20) of Fig. 5(b). In region II (Fig. 5(c)), only one measurement was obtained (objective X20), from the inner border of the tissue sample, corresponding to the myocardium-endocardium (purple circle in Fig. 5(c)). The obtained HRmBS peaks are shown together in Fig. 5(d). Figure 5(e) shows the Anti-Stokes side in order to make the details more

Biomedical Optics EXPRESS

visible (lines are only guides to the eyes) and Fig. 5(f) is an example of a typical fit of the experimental data. Quantifications of Brillouin spectroscopy of the three different heart layers were performed. Frequency shift (f) and half width at half maximum (HWHM) that corresponds to the hypersonic attenuation (Γ) of the Brillouin peak were derived from the fit analysis of the spectra: A) f = 17.01 ± 0.02 GHz; HWHM = 0.64 ± 0.06 GHz. B) f = 17.39 ± 0.01 GHz; HWHM = 0.57 ± 0.06 GHz. C) f = 17.51 ± 0.03 GHz; HWHM = 0.67 ± 0.06 GHz.

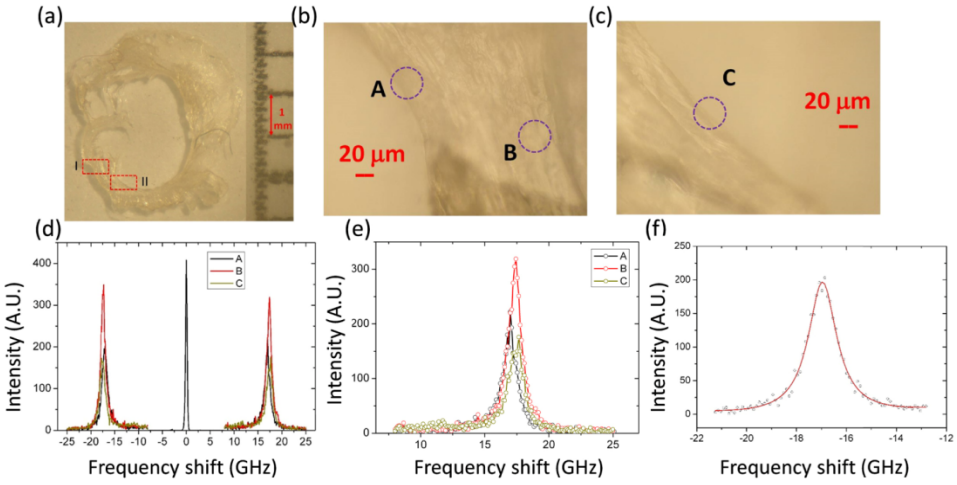

Fig. 5. Brillouin spectroscopy for different histological layers of the heart. (a) Optical image of cleared transversal heart cross-section were acquired with a Stereolupe. (b, c) Magnification of the areas I and II respectively and analysed with Brillouin spectroscopy. IA, epicardial layer; IB, myocardium; IIC, endocardium. Optical images were acquired with a 20X objective. The purple circles represent the area of the scattering volume. These areas result bigger than expected due to very high elastic scattering on the tissue surface. (d, e) Brillouin scattering spectrum of the three indicated areas in (B) and (C). Different colours represent the different tissue areas (A, B and C). (f) Result of a non linear squares fit (red line) of the experimental data (circles) using a simple lorentzian function plus a suited background function for the stokes side of the Brillouin spectrum of the A region shown in Fig. 5(e).

These results evidence the power of the HRmBS technique in order to assess differences in mechanical properties of different regions of cleared heart tissue. In order to assess the homogeneity of these regions, a Brillouin frequency shift map about the epicardial-myocardial layer was obtained. A region of 50x30 µm2 was mapped in 10 µm steps using the X20 microscope objective. The green rectangle in Figs. 6(a) and 6(b) is the mapped zone. To enhance the contrast of the micrograph, Fig. 6(a) was obtained using crossed polarizers, while Fig. 6(b) was a standard micrograph. The results for the Brillouin frequency shift and hypersonic attenuation (Half Width at Half Maximum, HWHM) of the HRmBS peaks are summarized in the maps of Figs. 6(c) and 6(d) respectively. Despite the rough resolution of the maps, it is very easy to see the frontier between the tissue sample region and the region without tissue (brown and black regions in the maps). Inside the tissue, frequency variations are small, and in absolute value remain very close to the value obtained in region A (Fig. 5(b)) and far from the value obtained in region B (Fig. 5(b)). Only two points seem to disagree, but is only due to the fact that the HRmBS peak was statistically poor as in the scattering volume there was only a small portion of tissue sample and the peak intensity obtained was very faint.

Biomedical Optics EXPRESS

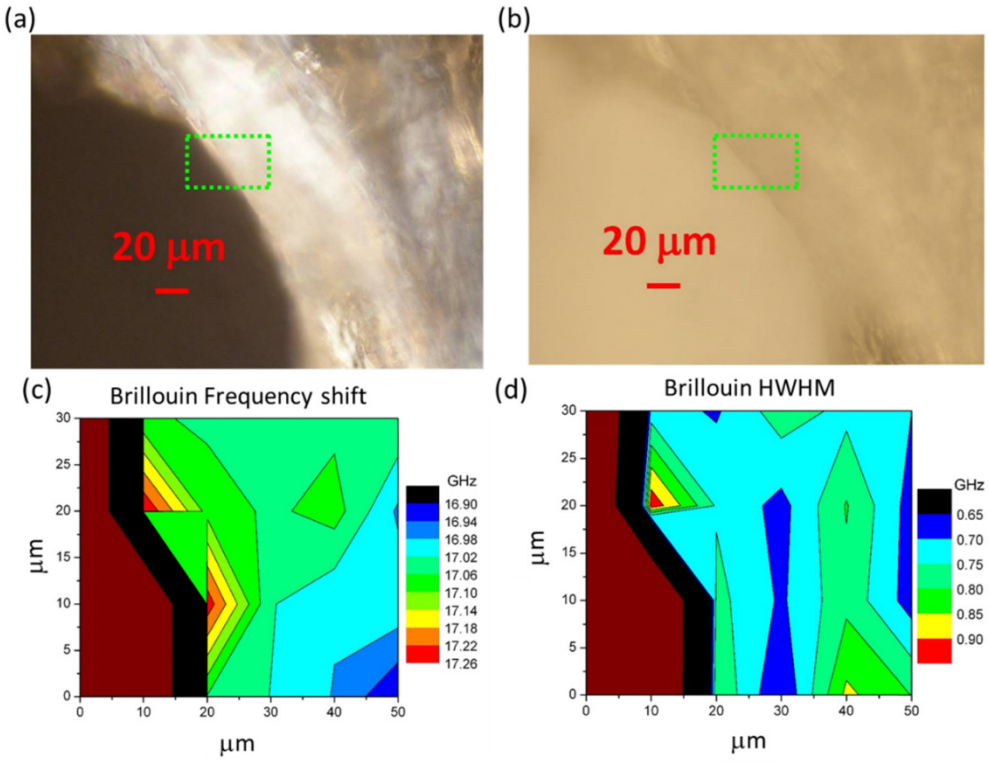

Fig. 6. Brillouin spectroscopy map of cleared heart sections. (a, b) Optical images of heart cross-section with (a) and without (b) crossed polarizers obtained with a 20X objective. (c, d) Colour maps showing the spatial distribution of the Brillouin frequency shift and hypersonic attenuation of the scanned area respectively. The dimension of the scanned matrix is 50x30 µm2 with spectra recorded in 10 µm steps and with a 20X objective. Brown and black areas indicate the frontier region, in which there were no peaks. The first peak measured was at the left inferior corner and the last one was at the right superior corner.

The HWHM map shown in Fig. 6(d) presents slightly more variability of the experimental values, but still within expected range for complex biological tissues.

4. Conclusion

In this work we have explored for the first time the combination of optical tissue clearing with high resolution micro-Brillouin spectroscopy for biological applications. We found that making the tissue transparent by using the CUBIC protocol, the HRmBS peaks clearly improved reliability without altering their positions, i.e., the mechanical properties of the tissues. Moreover, HRmBS has proven its suitability to detect small changes in mechanical properties of biological tissues. The possibility to make biological tissues transparent opens new analytical options that may bring biomechanics into the clinic in the future, specifically it could be used for the diagnosis of pathological conditions, for example in cardiovascular diseases.

Funding

Ministerio de Ciencia, Innovación y Universidades, the Pro CNIC Foundation, Severo Ochoa Center of Excellence (SEV-2015-0505); ISCIII-FIS grants PI18/00462 co-financed by ERDF, European Union (FEDER) Funds from the European Commission, European Union, "A way of making Europe"; MINECO/FEDER (MAT2015-65356-C3-1-R); Comunidad de Madrid

Biomedical Optics EXPRESS

(PHAMA 2.0-CM S2013/MIT-2740); CIBER de Salud Mental (CIBERSAM) and COST-action CA16124.

Acknowledgments

We are grateful to Elísabet Bello for assisting with the perfusion experiments. All experimental procedures were conducted in conformity with European Union Directive 2010/63/EU and were approved by the Ethics Committee for Animal Experimentation of hospital (Comité de Ética en Experimentación Animal, CEEA; number ES280790000087).

Disclosures

The authors declare that they have no conflict of interest.

References

1. S. H. Yun and D. Chernyak, "Brillouin microscopy: assessing ocular tissue biomechanics," Curr. Opin. Ophthalmol. **29**(4), 299–305 (2018).
2. J. M. Vaughan and J. T. Randall, "Brillouin scattering, density and elastic properties of the lens and cornea of the eye," Nature **284**(5755), 489–491 (1980).
3. F. Palombo, M. Madami, N. Stone, and D. Fioretto, "Mechanical mapping with chemical specificity by confocal Brillouin and Raman microscopy," Analyst (Lond.) **139**(4), 729–733 (2014).
4. F. Palombo, M. Madami, D. Fioretto, J. Nallala, H. Barr, A. David, and N. Stone, "Chemico-mechanical imaging of Barrett's oesophagus," J. Biophotonics **9**(7), 694–700 (2016).
5. R. S. Edginton, S. Mattana, S. Caponi, D. Fioretto, E. Green, C. P. Winlove, and F. Palombo, "Preparation of Extracellular Matrix Protein Fibers for Brillouin Spectroscopy," J. Vis. Exp. (115), (2016).
6. S. Mattana, S. Caponi, F. Tamagnini, D. Fioretto, and F. Palombo, "Viscoelasticity of amyloid plaques in transgenic mouse brain studied by Brillouin microspectroscopy and correlative Raman analysis," J. Innov. Opt. Health Sci. **10**(6), 1742001 (2017).
7. S. Corezzi, L. Comez, and M. Zanatta, "A simple analysis of Brillouin spectra from opaque liquids and its application to aqueous suspensions of poly-N-isopropylacrylamide microgel particles," J. Mol. Liq. **266**, 460–466 (2018).
8. G. Scarcelli and S. H. Yun, "Confocal Brillouin microscopy for three-dimensional mechanical imaging," Nat. Photonics **2**(1), 39–43 (2007).
9. K. Elsayad, S. Werner, M. Gallemí, J. Kong, E. R. Sánchez Guajardo, L. Zhang, Y. Jaillais, T. Greb, and Y. Belkhadir, "Mapping the subcellular mechanical properties of live cells in tissues with fluorescence emission-Brillouin imaging," Sci. Signal. **9**(435), rs5 (2016).
10. G. Antonacci and S. Braakman, "Biomechanics of subcellular structures by non-invasive Brillouin microscopy," Sci. Rep. **6**(1), 37217 (2016).
11. R. Schlüßler, S. Möllmert, S. Abuhattum, G. Cojoc, P. Müller, K. Kim, C. Möckel, C. Zimmermann, J. Czarske, and J. Guck, "Mechanical Mapping of Spinal Cord Growth and Repair in Living Zebrafish Larvae by Brillouin Imaging," Biophys. J. **115**(5), 911–923 (2018).
12. Z. Steelman, Z. Meng, A. J. Traverso, and V. V. Yakovlev, "Brillouin spectroscopy as a new method of screening for increased CSF total protein during bacterial meningitis," J. Biophotonics **8**(5), 408–414 (2015).
13. T. Yu, Y. Qi, H. Gong, Q. Luo, and D. Zhu, "Optical clearing for multiscale biological tissues," J. Biophotonics **11**(2), e201700187 (2018).
14. A. Feuchtinger, A. Walch, and M. Dobosz, "Deep tissue imaging: a review from a preclinical cancer research perspective," Histochem. Cell Biol. **146**(6), 781–806 (2016).
15. F. Palombo, F. Masia, S. Mattana, F. Tamagnini, P. Borri, W. Langbein, and D. Fioretto, "Hyperspectral analysis applied to micro-Brillouin maps of amyloid-beta plaques in Alzheimer's disease brains," Analyst (Lond.) **143**(24), 6095–6102 (2018).
16. E. A. Susaki, K. Tainaka, D. Perrin, F. Kishino, T. Tawara, T. M. Watanabe, C. Yokoyama, H. Onoe, M. Eguchi, S. Yamaguchi, T. Abe, H. Kiyonari, Y. Shimizu, A. Miyawaki, H. Yokota, and H. R. Ueda, "Whole-brain imaging with single-cell resolution using chemical cocktails and computational analysis," Cell **157**(3), 726–739 (2014).
17. E. A. Susaki, K. Tainaka, D. Perrin, H. Yukinaga, A. Kuno, and H. R. Ueda, "Advanced CUBIC protocols for whole-brain and whole-body clearing and imaging," Nat. Protoc. **10**(11), 1709–1727 (2015).
18. E. A. Susaki, K. Tainaka, D. Perrin, F. Kishino, T. Tawara, T. M. Watanabe, C. Yokoyama, H. Onoe, M. Eguchi, S. Yamaguchi, T. Abe, H. Kiyonari, Y. Shimizu, A. Miyawaki, H. Yokota, and H. R. Ueda, "Whole-brain imaging with single-cell resolution using chemical cocktails and computational analysis," Cell **157**(3), 726–739 (2014).
19. I. Nehrhoff, D. Bocancea, J. Vaquero, J. J. Vaquero, J. Ripoll, M. Desco, and M. V. Gómez-Gaviro, "3D imaging in CUBIC-cleared mouse heart tissue: going deeper," Biomed. Opt. Express **7**(9), 3716–3720 (2016).
20. I. Nehrhoff, J. Ripoll, R. Samaniego, M. Desco, and M. V. Gómez-Gaviro, "Looking inside the heart: a see-through view of the vascular tree," Biomed. Opt. Express **8**(6), 3110–3118 (2017).

Biomedical Optics EXPRESS

21. M. V. Gómez-Gaviro, E. Balaban, D. Bocancea, M. T. Lorrio, M. Pompeiano, M. Desco, J. Ripoll, and J. J. Vaquero, "Optimized CUBIC protocol for three-dimensional imaging of chicken embryos at single-cell resolution," Development **144**(11), 2092–2097 (2017).
22. R. J. Jiménez Riobóo, V. Brien, and P. Pigeat, "Elastic properties in different nano-structured AlN films," J. Mater. Sci. **45**(2), 363–368 (2010).
23. J. R. Sandercock, *Trends in Brillouin Scattering: Studies of Opaque Materials, Supported Films, and Central Modes* (Springer-Verlag, Berlin, Heidelberg, 1982).
24. R. Vacher and L. Boyer, "Brillouin Scattering: A Tool for the Measurement of Elastic and Photoelastic Constants," Phys. Rev. **6**(2), 639–673 (1972).
25. J. K. Küger, *Optical Techniques to Characterize Polymer Systems in Studies in Polymer Science* (Elsevier Amsterdam, 1989).
26. P. J. Wu, I. V. Kabakova, J. W. Ruberti, J. M. Sherwood, and I. E. Dunlop, "Water content, not stiffness, dominates Brillouin spectroscopy measurements in hydrated materials," **15**, 561–562 (2018).
27. E. Posada, M. J. Roldán-Ruiz, R. J. Jiménez Riobóo, M. C. Gutiérrez, M. L. Ferrer, and F. del Monte, "Nanophase separation in aqueous dilutions of a ternary DES as revealed by Brillouin and NMR spectroscopy," J. Mol. Liq. **276**, 196–203 (2019).